Available online at www.sciencedirect.com
ScienceDirect
Catalysis Today 117 (2006) 234–241
CATALYSIS TODAY
www.elsevier.com/locate/cattod

New Cs-containing Mo–V^{4+} based oxides with the structure of the M1 phase—Base for new catalysts for the direct alkane activation

H. Hibst [a,*], F. Rosowski [a], G. Cox [b]

[a] *BASF Aktiengesellschaft, Chemicals Research and Engineering, D-67056 Ludwigshafen, Germany*
[b] *BASF Aktiengesellschaft, Polymer Research, D-67056 Ludwigshafen, Germany*

Available online 13 July 2006

Abstract

The high catalytic performance of $Mo_{3.5}V^{4+}W_{0.5}O_{14}$ for the selective oxidation of acrolein (ACR) to acrylic acid (AA) is strongly connected to its semi-crystalline tunnel structure of an oxidic bronze. The real structure in the crystallographic (*a* and *b*)-plane is characterized by an intergrowth of different channel sizes typical for oxidic bronze structures without long-range order in the (*a* and *b*)-plane. The growth direction of the needle-shaped crystals is perpendicular to the (*a* and *b*)-plane and parallel to the crystallographic *c*-axis. In this direction, in contrast to the high disorder of different tunnel motifs in the (*a* and *b*)-plane, a strong crystallographic order of corner-shared MO_6 octahedra (M = Mo, V, W) is observed. A structural analogue in the family of the block or shear structures is M-Nb_2O_5. This structure is characterized by an intimate intergrowth of ReO_3-blocks with very different block sizes and without any long-range order in the (*a* and *b*)-plane, and by a high order of corner-shared NbO_6 octahedra in [*c*].

The semi-crystalline oxidic bronze structure of $Mo_{3.5}V^{4+}W_{0.5}O_{14}$ is not unique. Many ternary and quaternary oxides of transition metals, which crystallize at high temperatures with the crystal structure of oxidic bronzes, at low calcination temperatures exhibit a semi-crystalline bronze structure.

$Mo_{10}V_2{}^{4+}Nb_2TeO_{42-x}$ with the crystal structure of $Cs_{0.5}[Nb_{2.5}W_{2.5}O_{14}]$ (M1 phase) exhibits its best catalytic properties in the direct oxidation of propane to acrylic acid if no impurity of M2 phase is present. Phase-pure M1 phase can be prepared in a highly reproducible way by avoiding any precipitation by continuous and instantaneous spray-drying of aqueous solutions. The resulting amorphous precursor is calcinated in air (<300 °C) and in N_2 (300–650 °C) and post-treated with aqueous acids to remove any impurity of undesired phases (e.g. the M2 phase).

New Mo–V based oxides with the composition $A_{0.5}[Mo_{5-a-b}V_a{}^{4+}X_bO_{14}]$ (A = Rb, Cs, X = no element, Nb, Ta, W, Sb, Bi, Se, Te, . . .) and with the structure of the M1 phase can be prepared. Due to the Cs-content, the new compounds exhibit a low catalytic activity in the direct propane oxidation. By treating $Cs_{0.5}[Mo_{3.7}V_{1.2}{}^{4+}Bi_{0.1}O_{13.9}]$ with $HClO_4$ 50% of the Cs could be removed, and the catalytic activity was increased. Therewith the mentioned new preparation concept for tailor-made new Mo–V based M1 phases with limited Cs-content and with flexible composition may enable new and well-defined M1 phases with (e.g. Bi containing) active sites to overcome the catalytic difficulties in the step of the oxidative transformation of propene to acrolein within the direct oxidation of propane to AA.

Keywords: Mo–V oxides; M1 phase; Stabilization; Cs–Nb–W–O; Cs–Mo–V–X–O; Mo–V–Nb–Te–O; Acrylic acid

1. Introduction

Mo–V based oxidic compositions with a Mo/V ratio of larger than 1 are the basis for several high performance heterogeneous catalysts, e.g. for the selective oxidation of propane or acrolein (ACR) to acrylic acid (AA) or for the oxidation of ethane to ethene or to acetic acid in the gas phase [1–3]. Semi-crystalline Mo–V–W–O is the preferred active phase for the oxidation of ACR to AA, while highly crystalline Mo–V–Nb–Te–O leads to the highest AA yields concerning the direct oxidation of propane to AA [15,16]. It is known that the structure of $Cs_{0.5}[Nb_{2.5}W_{2.5}O_{14}]$ resembles strongly the M1 phase of Mo–V–Nb–Te–O. Calcination experiments at lower temperatures show that Cs–Nb–W–O can be prepared with the semi-crystalline structure too. The high stability of this compound enables a TEM-investigation of the semi-crystalline structure type. Furthermore, new Cs-containing Mo–V^{4+} based oxides with the crystal structure of Mo–V–Nb–Te–O and prospective catalytic properties for different catalytic oxidation reactions will be introduced.

* Corresponding author.
E-mail address: hartmut.hibst@basf.com (H. Hibst).

0920-5861/$ – see front matter © 2006 Elsevier B.V. All rights reserved.
doi:10.1016/j.cattod.2006.05.045

2. Semi-crystalline Mo–V–W oxide

Mo–V based oxidic compositions for the selective oxidation of ACR to AA have been invented in the sixties by a Scottish Whisky distillery [1]. In the following years, beneath Cu additional transition elements like W or Nb have been introduced into the catalyst. Today Mo–V–W–O based catalysts convert ACR at 250–300 °C into AA with nearly 100% conversion with an AA selectivity of more than 95% [4].

In 1978 Thorsteinson from Union Carbide Corp. noticed that the ''specific activity of $Mo_{0.6}V_{0.3}Nb_{0.1}O_x$ for the oxidehydrogenation of ethane to ethene is proportional to the intensity of its 4.00 Å reflection'', a sharp peak in the X-ray diffraction pattern at $2\Theta = 22.2^\circ$ (Cu-radiation) [2]. Andrushkevich found that the oxidation number of the V in mixed Mo–V oxides with an optimum catalytic performance is 4+ and the structure of the mixed oxide was suggested to be Mo_4O_{11} [3]. Our own investigations on the composition $Mo_{3.5}V^{4+}W_{0.5}O_{14}$ show that under optimum preparation conditions a monophasic semi-crystalline $Mo_{3.5}V^{4+}W_{0.5}O_{14}$ can be synthesized which is characterized by a very specific XRD pattern containing both sharp and broad diffraction peaks (Fig. 1) [4]. The preparation starts with a clear, aqueous solution of ammonium heptamolybdate (AHM), ammonium metavanadate (AMV) and ammonium paratungstate'' (APT). The orange-coloured solution containing mixed isopolyoxoanions with a homogenous distribution of Mo, V and W [5] is spray-dried. The resulting X-ray amorphous spray-dried powder is calcinated under optimum redox conditions of the gas phase up to 400 °C. The oxidation state of the V in the semi-crystalline $Mo_{3.5}V^{4+}W_{0.5}O_{14}$ (Fig. 1) is analytically controlled by potentiometric titration [4]. If the oxidation potential of the gas phase is too low, which may correspond to a very high concentration of NH_3 from the decomposition of the ammonium-containing precursors, the formation of $Mo_{0.95}V_{0.95}{}^{4+}O_5$ [6] and MoO_2 is observed. On the other hand, if the oxidation potential of the gas phase is too high, e.g. due to a high concentration of O_2, $Mo_{0.87}V_{0.13}{}^{5+}O_{2.935}$ is formed [7] with the hexagonal structure of MoO_3. Thermal treatment of $Mo_{3.5}V^{4+}W_{0.5}O_{14}$ at temperatures >500 °C leads to a crystallization into the crystal structure of Mo_5O_{14} [8] with insufficient catalytic properties.

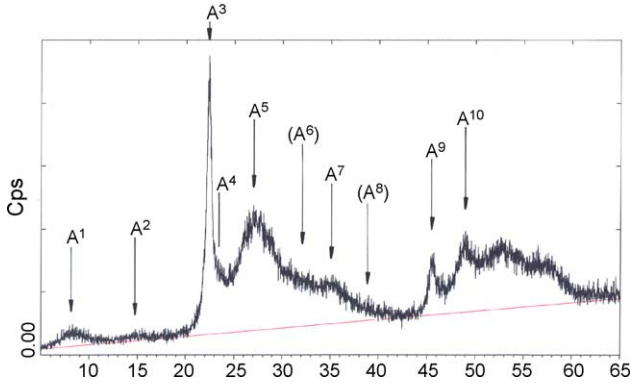

Fig. 1. XRD pattern of semi-crystalline $Mo_{3.5}V^{4+}W_{0.5}O_{14}$ for the selective oxidation of acrolein to acrylic acid (x-axis: 2θ (°); y-axis: intensity). The peak with the highest intensity corresponds to $d = 4.0$ Å.

The semi-crystalline $Mo_{3.5}V^{4+}W_{0.5}O_{14}$ prepared at 400 °C consists of nanoparticles with needle-shape (average length ≈ 50–100 nm; thickness ≈ 10–20 nm). The structural investigation by HR-TEM shows, that the MO_6-octahedra (M = Mo, V, W) are corner-shared in the direction of the crystallographic c-axis which gives rise to a short c-axis of 0.4 nm and a sharp peek in the XRD pattern at $2\theta = 22.2^\circ$ in Fig. 1. The crystallographic c-axis is identical with the growth direction of the crystals and therewith with the needle-axis of the nanoparticles. The TEM-investigation of the crystal structure vertical to the growth direction of the needles in the (a and b)-plane is difficult, due to the low stability of the mixed oxide under the investigating electron beam. Although the W content of the oxide leads to a certain stabilization of the structure, until now no clear visualization by TEM of the real structure of Mo–V–X oxides (X = W, Nb) was possible. Low dose TEM-investigations came to the preliminary conclusion, that the semi-crystalline Mo–V based oxide is a ''Mo_5O_{14}-type Mo–V–W oxide'' [9–14]. Based on new investigations of the thermally more stable system Cs–Nb–W–O it now is possible to investigate the real structure of semi-crystalline oxides with an XRD pattern shown in Fig. 1 by HR-TEM. The investigation shows that the real structure is characterized by an intergrowth of different oxidic bronze structures with different channel sizes and without any long-range order in the (a and b)-plane. This will be shown more clearly in Section 4 (Figs. 6 and 7).

3. Highly crystalline Mo–V^{4+} oxides

The catalytic system Mo–V–Nb–Te–O was invented for the direct (amm)oxidation of propane into acrylonitrile or AA in the early nineties by Ushikubo, Mitsubishi Chem. Corp. [15,16]. For the conversion of propane into AA a yield of 48.5% was published [16] ($C_{Propane} = 80.1\%$, $S_{AA} = 60.5\%$; propane:air:H_2O = 1:15:14, $T = 380$ °C, SV = 1.861 h^{-1}). The claimed crystal structure of the catalyst is the hexagonal M2 phase and this probably gave rise to problems in reproducing the catalytic results by others later on. Our experiments show that the catalytic performance of the catalyst strongly depends on its crystal structure and that the only crystal phase, which can accelerate the direct oxidation of propane into AA is the orthorhombic M1 structure [20–22].

An optimized and highly reproducible preparation procedure of the M1 phase starts with two aqueous solutions of the components (solution A containing AHM, AMV and telluric acid, solution B containing Nb oxalate). These are mixed instantaneously and continuously with a typical composition $MoV_{0.30}Nb_{0.12}Te_{0.23}O_x$. The resulting clear, aqueous solution is spray-dried before a precipitate is observed [17]. The resulting product is an X-ray amorphous powder. The structural and catalytic performance of the M1 phase of Mo–V–Nb–Te–O profits from the same preparation conditions adopted in the preparation of the semi-crystalline Mo–V–W–O (Section 2). That means that the calcination of the amorphous spray-dried powder must be adapted in a gas phase with a redox potential

adequate for vanadium(IV). In an optimum calcination procedure at low temperatures (<300 °C) the ammonium and oxalate components are decomposed in the presence of air, while the calcination at higher temperature proceeds under an inert gas like N_2. It is noticeable that, calcination at 400 °C leads to a semi-crystalline Mo–V–Nb–Te oxide with the XRD pattern shown in Fig. 1. If the calcination temperature is further increased to 650 °C, the M1 phase can be prepared with a high crystallinity and with high AA yields. In most cases a small addition of the M2 phase is observed in the calcination products. A further increase in calcination temperature to >700 °C leads to the crystal structure of Mo_5O_{14} with an unsatisfying catalytic performance.

The identification and quantification of the M1 and M2 phase in the samples prepared at 650 °C is carried out by electron micro-diffraction in the TEM. Elongated crystals usually exhibit the selected area diffraction (SAD)-pattern of the orthorhombic M1 structure while larger platelets with particle diameters of some micrometers show the SAD-pattern of the hexagonal M2 phase. The analysis of the composition of the different phases in the TEM by energy dispersive X-ray spectroscopy (EDXS) shows that the M1 phase ($Mo_{71}V_{13}Nb_{13}Te_3O_x$) contains significantly more Nb than the M2 phase ($Mo_{58}V_{20}Nb_5Te_{17}O_x$) with a high Te-content. Therewith the M1 and the M2 phase do not only distinguish by their crystal structure but also by their composition.

To improve the catalytic performance of the samples prepared at 650 °C and containing mainly the M1 phase and additionally small amounts of the M2 phase, these samples are preferably post-treated with aqueous acids (e.g. with 30% HNO_3), which leads to a selective dissolution of the undesired M2 phase [18,19]. The M1 phase purified by this way has the composition $Mo_{10}V_2^{4+}Nb_2TeO_{42-x}$ and a specific surface area of 10–20 m^2/g. It consists out of board- or tray-shaped, elongated crystals with an average length of about 1 μm and a thickness of 0.05–0.1 μm (Fig. 2). TEM-investigations show that the crystallographic

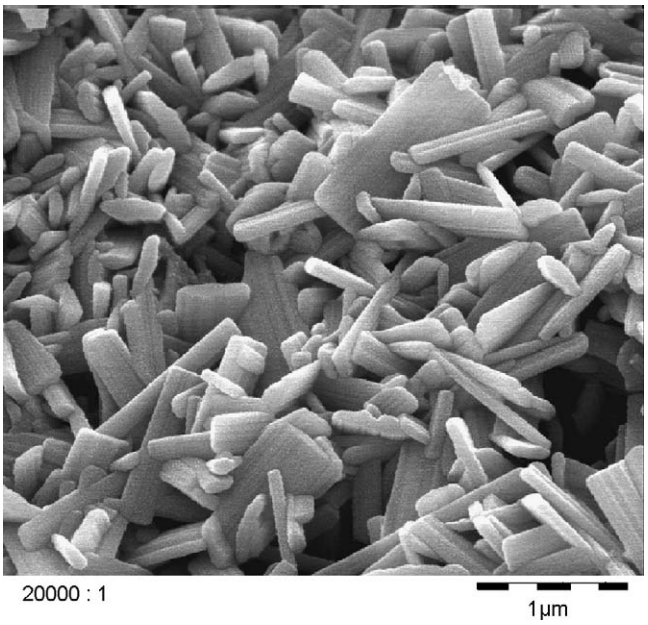

Fig. 2. Monophasic M1 phase, purified by treatment with an aqueous acid, with the composition $Mo_{10}V_2^{4+}Nb_2TeO_{42-x}$ and a specific surface area of 10 m^2/g. The powder consists of board- or tray-shaped, elongated crystals with an average length of 1 μm and a thickness of 0.05–0.1 μm. The crystallographic *c*-axis is oriented parallel to the needle-axis.

c-axis is oriented parallel to the board-axis. The HR-TEM lattice image of the (*a* and *b*)-plane of the M1 phase (Fig. 3) is consistent with the orthorhombic structure solved by former X-ray investigations [20–22]. XRD-investigations at the Synchrotron in Brookhaven, USA, exhibit that Te is build in the six-sided channels of the lattice [23]. This obviously leads to a significant stabilization of the M1 structure.

The M1 phase purified in the mentioned way by an acidic treatment shows an optimum in catalytic performance concerning the direct oxidation of propane to AA. In the step

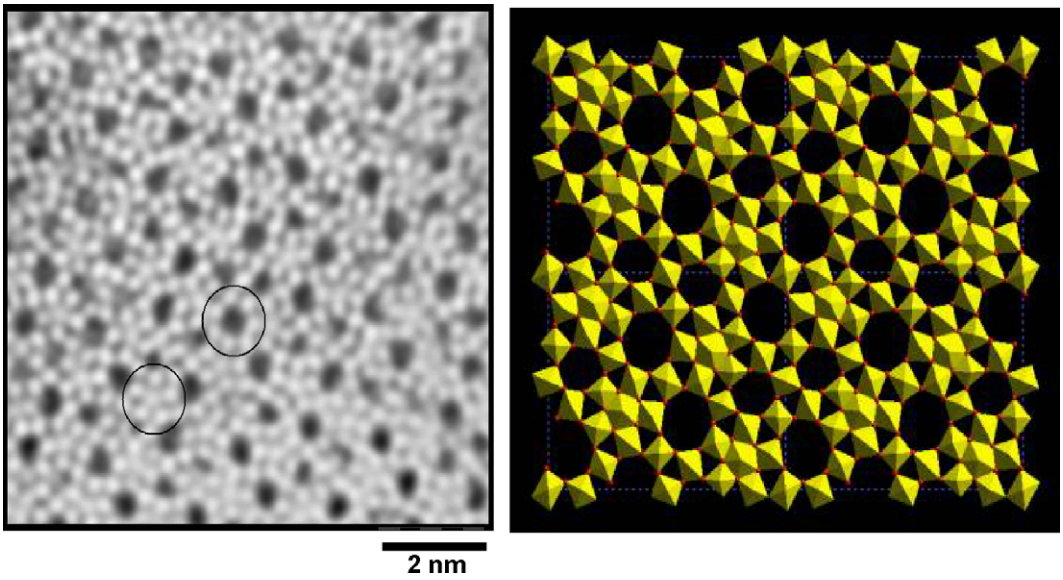

Fig. 3. The HR-TEM lattice image of the (*a* and *b*)-plane of the M1 phase is consistent with X-ray investigations [20–22].

of acid treatment not only the M2 phase is dissolved but also it must be assumed that the crystal surface of the M1 phase is partially etched. Etching preferably should remove a potentially amorphous surface layer. Therewith the fact that the acid-treatment leads to a significant improvement in catalysis does not support theories concerning an amorphous surface layer on Mo–V–Nb–Te–O to be essential for catalytic properties.

Other catalytic models only consider active sites on the (*a* and *b*)-plane of the orthorhombic M1 phase [24]. But a simple calculation shows that due to the extreme needle-shape of the particles the geometric surface area of the crystallographic (*a* and *b*)-plane evolves only about 5% of the total surface area of the crystals, and it is hard to believe that only this low surface area would contribute to the main part of catalysis.

It is noticeable that the XRD pattern of the highly crystalline M1 phase of $Mo_{10}V_2^{4+}Nb_2TeO_{42-x}$ for the direct oxidation of propane to AA shows very large similarities with the diffraction pattern of the semi-crystalline $Mo_{3.5}V^{4+}W_{0.5}O_{14}$ for the oxidation of ACR to AA (Fig. 4). To clarify the structural differences between the highly crystalline M1 phase and the semi-crystalline Mo–V–W–O (Figs. 1 and 4) or the presumably isostructural semi-crystalline Mo–V–Nb–Te–O observed at a low calcination temperature of 400 °C, investigations in the system Cs–Nb–W–O were undertaken.

4. Investigations in the system Cs–Nb–W–O and new Cs-containing Mo–V^{4+} based oxides with the structure of the M1 phase of Mo–V–Nb–Te–O

Aqueous suspensions containing Nb oxalate, APT and in most cases also Cs_2CO_3 with the composition $Cs_a[Nb_{2+a}W_{3-a}O_{14}]$ ($a = 0$, 0.25 and 0.5) are spray-dried and calcinated in air. A calcination temperature of 700 °C leads for all three compositions $Cs_0[Nb_2W_3O_{14}]$ (=$Nb_2W_3O_{14}$), $Cs_{0.25}[Nb_{2.25}W_{2.75}O_{14}]$ and $Cs_{0.5}[Nb_{2.5}W_{2.5}O_{14}]$ into the semi-crystalline structure (Fig. 5) with an XRD pattern which is very similar to the XRD pattern of the semi-crystalline Mo–V–W

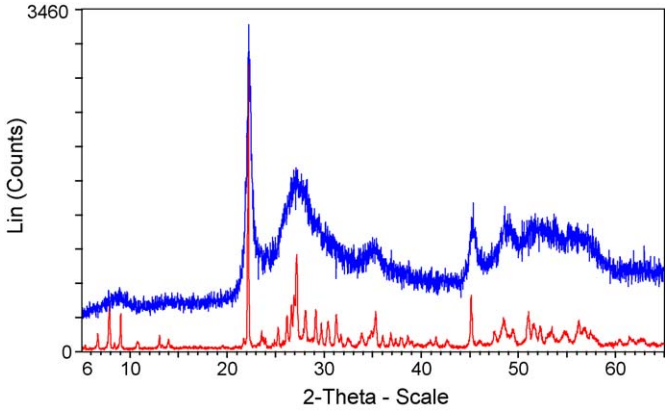

Fig. 4. The XRD pattern of the highly crystalline M1 phase with the composition $Mo_{10}V_2^{4+}Nb_2TeO_{42-x}$ for the direct oxidation of propane to acrylic acid (upper curve) shows very large similarities with the diffraction pattern of the semi-crystalline $Mo_{3.5}V^{4+}W_{0.5}O_{14}$ for the oxidation of acrolein to acrylic acid (lower curve) (*x*-axis: 2θ (°); *y*-axis: intensity). (For interpretation of the references to colour in this figure legend, the reader is referred to the web version of the article.)

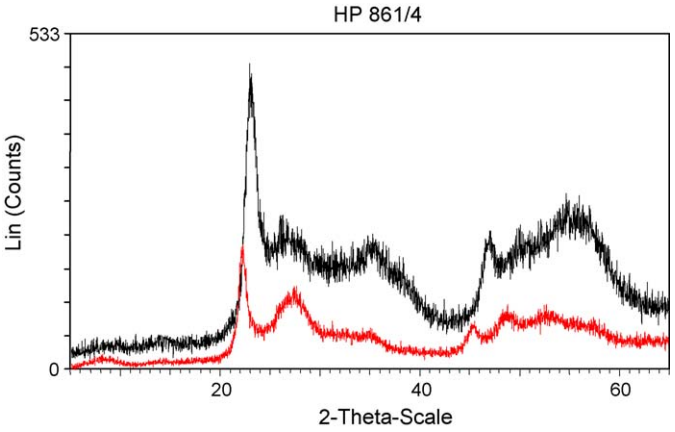

Fig. 5. XRD patterns of different semi-crystalline oxides (lower curve: $Mo_{3.5}V^{4+}W_{0.5}O_{14}$ (Fig. 1); upper curve: $Nb_2W_3O_{14}$, prepared by calcination (700 °C) of a spray-dried suspension containing Nb oxalate and APT) (*x*-axis: 2θ (°); *y*-axis: intensity). (For interpretation of the references to colour in this figure legend, the reader is referred to the web version of the article.)

oxide shown in Fig. 1. A higher calcination temperature of about 1000 °C converts the first composition $Cs_0[Nb_2W_3O_{14}]$ (=$Nb_2W_3O_{14}$) into the crystal structure of the oxidic bronze $Nb_8W_9O_{47}$ [25], the second composition $Cs_{0.25}[Nb_{2.25}W_{2.75}O_{14}]$ into the crystal structure of Mo_5O_{14} and the third composition $Cs_{0.5}[Nb_{2.5}W_{2.5}O_{14}]$ into the phase-pure crystal structure that is very similar to the structure of the M1 phase. The last result is consistent with TEM-investigations of Lundberg and Sundberg [26], who showed that the Cs-ions in $Cs_a[Nb_{2+a}W_{3-a}O_{14}]$ for $a \approx 0.5$ are accommodated in the six- and seven-sided tunnels of the bronze structure. It should be noted, that $Cs_{0.5}[Nb_{2.5}W_{2.5}O_{14}]$ and the M1 phase are almost isostructural. But precisely, in the case of M1, the coordinate of Te is $Z/C = 0.0$; however, in the case of $Cs_{0.5}[Nb_{2.5}W_{2.5}O_{14}]$ the coordinate of Cs is $Z/C = 0.5$.

On one hand, the experiments show that the semi-crystalline structure of the $Mo_{3.5}V^{4+}W_{0.5}O_{14}$ is not unique and presumably is formed at low calcination temperatures for a lot of oxides which generally are able to form oxidic bronze structures. On the other hand, it was shown that in the system Nb–W–O a small amount of Cs leads to a structural transformation into the Mo_5O_{14} structure, while larger amounts of Cs stabilize the oxidic bronze structure which resembles strongly the structure of the M1 phase.

Fortunately, the Cs ions stabilize the structure of the semi-crystalline $Cs_{0.5}[Nb_{2.5}W_{2.5}O_{14}]$ strongly. This for the first time enables the electron optical clarification of the real structure of the semi-crystalline structure by HR-TEM. This TEM-investigation of the semi-crystalline $Cs_{0.5}[Nb_{2.5}W_{2.5}O_{14}]$ (Fig. 6) and therewith of the presumably semi-crystalline $Mo_{3.5}V^{4+}W_{0.5}O_{14}$ in Fig. 1 leads to a typical tunnel structure of an oxidic bronze. Parallel to the *c*-axis and therewith parallel to the growth direction of the needle-shaped crystals a strong crystallographic order of MO_6 octahedra (M = Mo, V, W), shared at opposite corners in the direction of the *c*-axis, is observed. The real structure in the (*a* and *b*)-plane perpendicular to the *c*-axis is characterized by an intergrowth of different structural motifs of various oxidic bronze structures with different tunnel sizes and without any long-range order in the (*a* and *b*)-plane (Fig. 6).

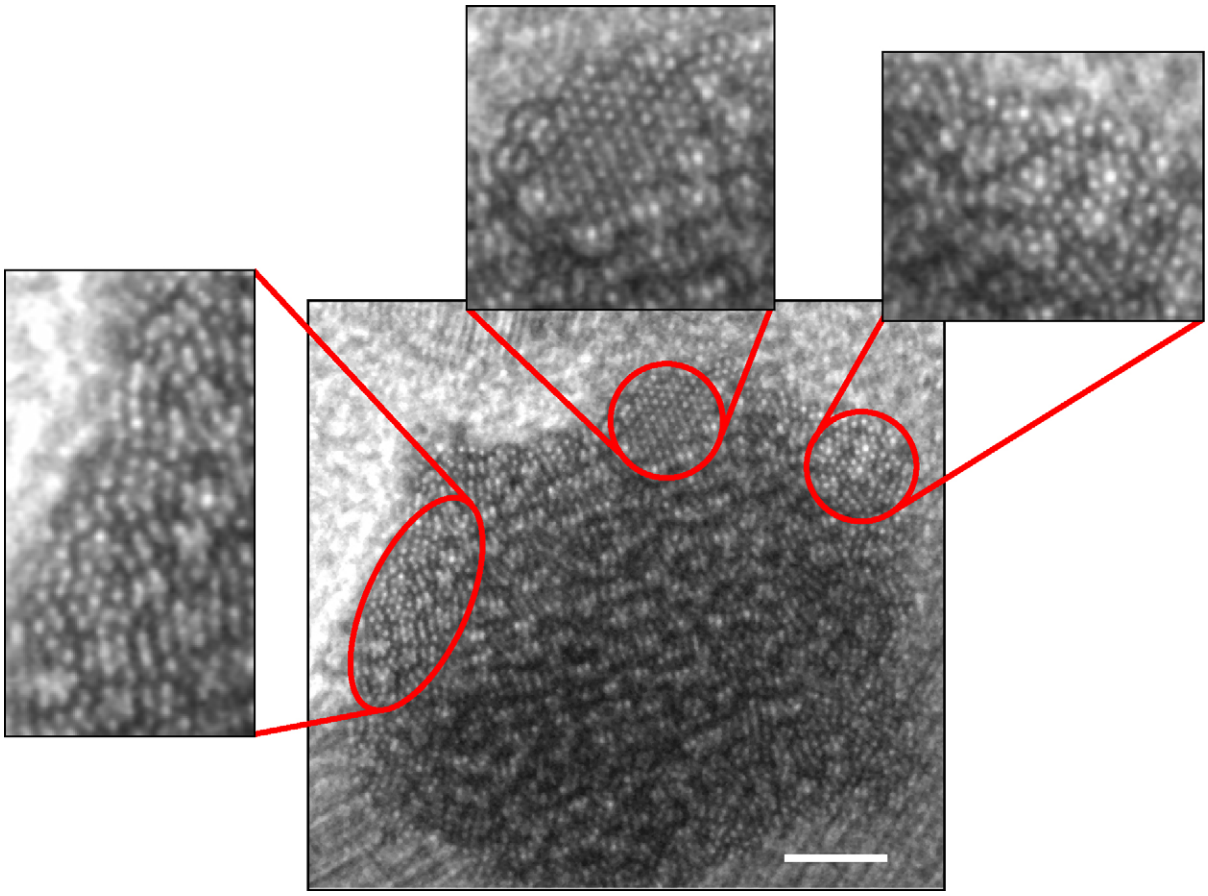

Fig. 6. HR-TEM-investigation of $Cs_{0.5}[Nb_{2.5}W_{2.5}O_{14}]$ prepared at 750 °C (*c*-axis perpendicular to the page surface, length bar = 10 nm). $Cs_{0.5}[Nb_{2.5}W_{2.5}O_{14}]$ in contrast to $Mo_{3.5}V^{4+}W_{0.5}O_{14}$ is stable under the electron beam of the TEM. The real structure in the (*a* and *b*)-plane is characterized by an intergrowth of different structural motifs of various oxidic bronze structures with different channel sizes and without any long-range order in the (*a* and *b*)-plane.

A sketch of the disordered tunnel structure in the (*a* and *b*)-plane is illustrated in Fig. 7.

Therewith a new and specific real structure with a tremendous crystallographic disorder in the (*a* and *b*)-plane and a strong crystallographic order in [*c*] has been identified within the family of the oxidic bronze structures. It should be mentioned that the analogue real structure in the family of the block or shear structures is M-Nb_2O_5 (Fig. 8) [27,28]. The structural motifs in this case are ReO_3-blocks of corner-shared NbO_6 octahedra. The ReO_3 blocks intergrow with different block sizes and without any long-range order in the crystallographic (*a* and *b*)-plane (Fig. 8).

At temperatures >900 °C $Cs_{0.5}[Nb_{2.5}W_{2.5}O_{14}]$ crystallizes with the similar structure of the M1 phase of $Mo_{10}V_2^{4+}Nb_2TeO_{42-x}$. High angle annular dark field-scanning transmission electron microscopy (HAADF-STEM) images of

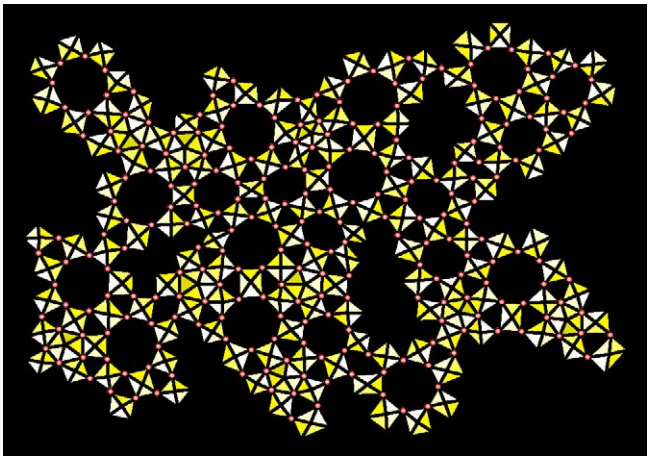

Fig. 7. Sketch of real structure of $Mo_{3.5}V^{4+}W_{0.5}O_{14}$ as identified by HR-TEM-investigation of isostructural $Cs_{0.5}[Nb_{2.5}W_{2.5}O_{14}]$ in the figure.

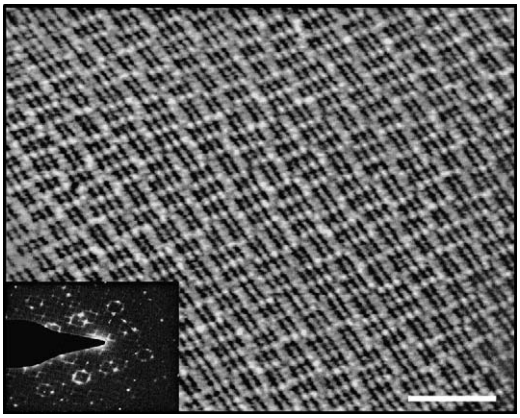

Fig. 8. Real structure of M-Nb_2O_5, structural analogue to semi-crystalline Mo–V oxides (HR-TEM-investigation, length bar = 5 nm).

the crystalline $Cs_{0.5}[Nb_{2.5}W_{2.5}O_{14}]$ (Fig. 9) show in agreement with TEM-investigations of Lundberg and Sundberg [26] that the Cs-ions are accommodated in the six- and seven-sided tunnels of the M1 structure (Fig. 10). An ab initio determination of the framework structure of the heavy-metal mixed oxide $Cs_{0.5}[Nb_{2.5}W_{2.5}O_{14}]$ from 100 kV precession electron diffraction data fit well with the result of a Rietveld refinement of X-ray powder data [29–31].

As mentioned in Section 3, Synchroton XRD measurements on $Mo_{10}V_2^{4+}Nb_2TeO_{42-x}$ confirm that Te ions are incorporated in the six-sided channels of the crystal lattice [23] stabilizing the M1 structure. In an analogous but more effective way the M1 phase of $Cs_{0.5}[Nb_{2.5}W_{2.5}O_{14}]$ is stabilized by Cs ions in the six- and seven-sided channels. Surprisingly, the utilization of this stabilization effect allows the preparation of new Mo–V based oxides with the composition $A_{0.5}[Mo_{5-a-b}V_aX_bO_{\approx 14}]$ and with the structure similar to the M1 phase. The stabilizing ion A in the Mo-rich compounds can be Rb oder Cs, while the lighter alkali ions exhibit no stabilizing effect concerning the M1 structure. The variable X is ''no element'' or, e.g. Nb, Ta, W, Sb, Bi, Se and/or Te [32]. An example for these new series of M1 phases for X = ''no element'' is $Cs_{0.5}[Mo_{3.8}V_{1.2}^{4+}O_{14.05}]$, for X = W is $Cs_{0.5}[Mo_{3.4}V_{1.2}^{4+}W_{0.4}O_{14}]$, for X = Te is $Cs_{0.5}[Mo_{3.5}V^{4+}Te_{0.5}O_{14-x}]$ (Fig. 11), for X = Nb and Te is $Cs_{1.5}[Mo_{10}V_2^{4+}Nb_2TeO_{42-x}]$, for X = Se is $Cs_{0.5}[Mo_{3.7}V_{1.2}^{4+}Se_{0.1}O_{14-x}]$, for X = Sb is $Cs_{0.5}[Mo_{3.5}V^{4+}Sb_{0.5}O_{14-x}]$ and for X = Bi is $Cs_{0.5}[Mo_{3.7}V_{1.2}^{4+}Bi_{0.1}O_{14-x}]$ (Fig. 12).

The solid phases are prepared by thermal treatment of an aqueous suspension containing Cs_2CO_3, AHM, AMV, metallic V powder and an additional, water-soluble compound of X at 90 °C for 12 h, subsequent spray-drying and calcination under N_2 atmosphere at 575–700 °C in dependence on the composition.

If these new solid phases are impregnated in a further step with phosphoric acid, the resulting catalysts in the gas phase oxidation of acrolein show unexpectedly high AA yields (>90%) [33]. Furthermore the P-promoted compounds with

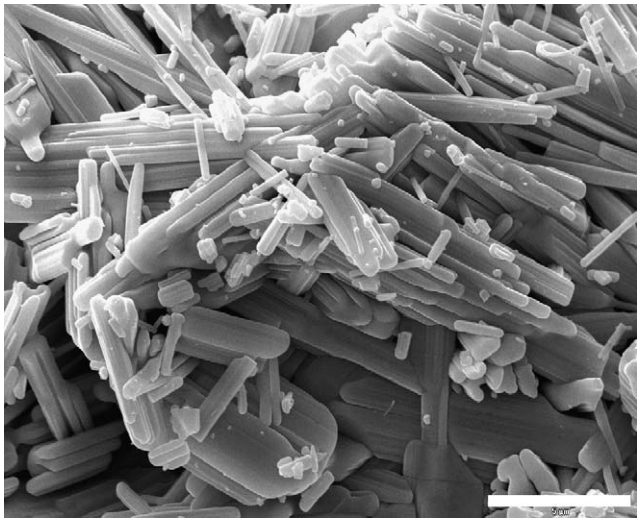

Fig. 9. Needle-shaped crystals of crystalline $Cs_{0.5}[Nb_{2.5}W_{2.5}O_{14}]$ prepared at 1000 °C (length bar = 1 μm).

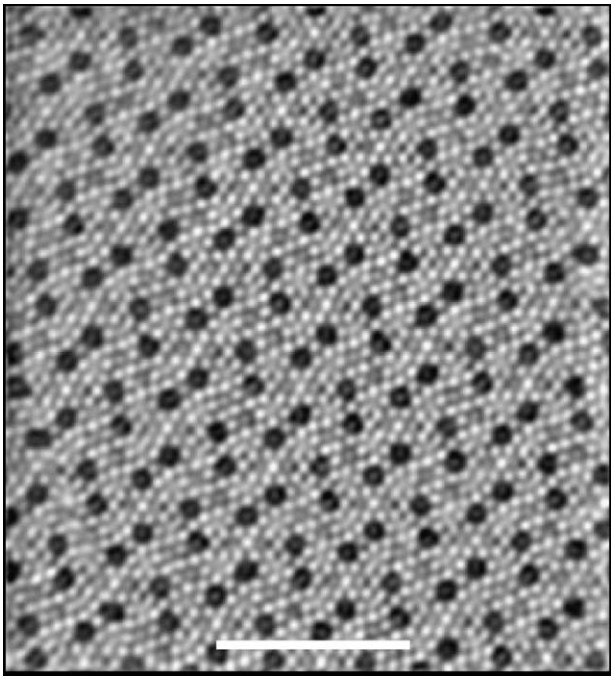

Fig. 10. High angle annular dark field-scanning transmission electron microscopy (HAADF-STEM) imaging of crystalline $Cs_{0.5}[Nb_{2.5}W_{2.5}O_{14}]$ prepared at 1000 °C (length bar = 5 nm). The real structure of $Cs_{0.5}[Nb_{2.5}W_{2.5}O_{14}]$ quite resemble the M1 phase of $Mo_{10}V_2^{4+}Nb_2TeO_{42-x}$. The structure is stabilized by Cs-ions within the six- and seven-sided tunnels [26,29–31].

X = Bi are very prospective new catalytic systems for the selective oxidation of methacrolein (MAC) to methacrylic acid (MAS). Therewith P-promoted catalysts $A_{0.5}[Mo_{5-a-b}V_aBi_bO_{\approx 14}]$ may compete in the future with the conventional catalytic systems for the oxidation of MAC to MAS containing heteropoly compounds with limited life-time under production conditions [34].

On the other hand, the new compounds are very prospective candidates for the direct (amm)oxidation of propane to AA or acrylonitrile. $Cs_{0.5}[Mo_{3.7}V_{1.2}^{4+}Bi_{0.1}O_{14-x}]$ is of special interest, because Bi is known to catalyze the oxidative conversion of propene to ACR, which in the direct

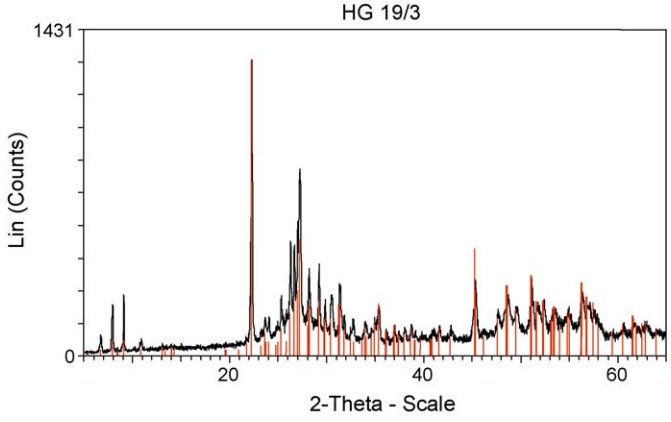

Fig. 11. XRD pattern of $Cs_{0.5}[Mo_{3.5}V^{4+}Te_{0.5}O_{14-x}]$ with the structure of the M1 phase, prepared by calcination of a spray-dried aqueous suspension of Cs_2CO_3, AHM, AMV, metallic V powder and H_6TeO_6 at 600 °C (6 h) in N_2 (*x*-axis: 2*θ* (°); *y*-axis: intensity).

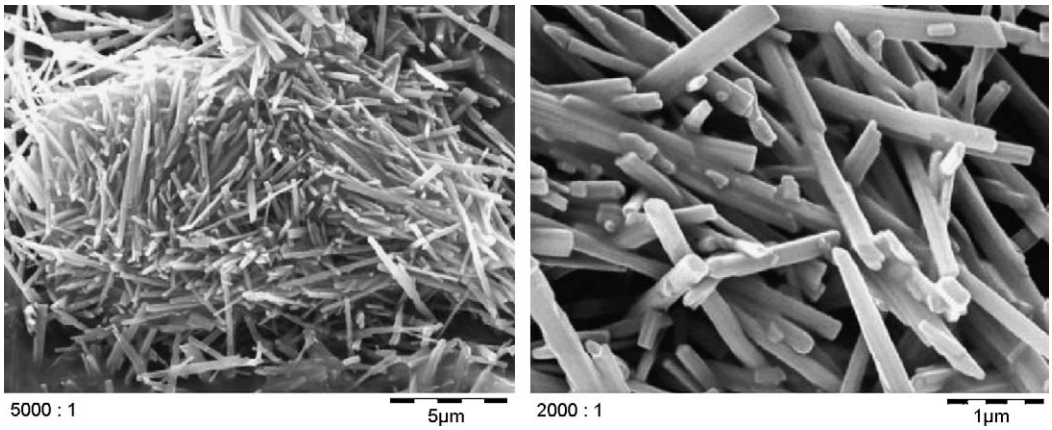

Fig. 12. Crystals of $Cs_{0.5}[Mo_{3.7}V_{1.2}{}^{4+}Bi_{0.1}O_{14-x}]$ prepared by calcination of a spray-dried aqueous suspension of Cs_2CO_3, AHM, AMV, metallic V powder and Bi nitrate at 600 °C (6 h) in N_2 [32].

oxidation of propane to AA is the mostly hindered step [35]. But due to their relatively high Cs-content the new compounds $A_{0.5}[Mo_{5-a-b}V_aX_bO_{\approx 14}]$ show a very low catalytic activity in the direct propane oxidation. To increase the acidity an exchange of the Cs ions against protons, ammonium or less basic elements, e.g. Li, may be valuable. In first experiments $Cs_{0.5}[Mo_{3.7}V_{1.2}{}^{4+}Bi_{0.1}O_{14-x}]$ was treated at 80 °C for 10 h with the strong acid $HClO_4$, and it was possible to remove 50% of the Cs-ions. As a result, the catalytic activity in the direct oxidation of propane to AA increased significantly. Other ways to increase the acidity of the new compounds by decreasing their Cs content may be leaching with other solvents, melts or complexing agents.

Therewith the mentioned new preparation concept for tailor-made new compounds of the Mo–V based M1 phase family with limited Cs-content and with flexible composition may enable new and well-defined M1 phases with, e.g. Bi and Fe containing active sites to overcome in the direct oxidation of propane to AA the catalytic difficulties in the step of the oxidative transformation of propene to acrolein.

References

[1] J.R. Bethell, E.J. Gasson, D.J. Hadley, R.F. Neale, The Destillers Comp. Ltd., Patent GB 903 034, publ. 09.08.1962.
[2] E.M. Thorsteinson, T.P. Wilson, F.G. Young, P.H. Kasai, J. Catal. 52 (1978) 116.
[3] T.V. Andrushkevich, L.M. Plyasova, G.G. Kuznetsova, V.M. Bondareva, T.P. Gorshkova, I.P. Olenkova, N.I. Lebedeva, React. Kinet. Catal. Lett. 12 (1979) 463.
[4] H. Hibst, A. Tenten, L. Marosi, BASF Aktiengesellschaft, Patent EP 774 297, publ. 21.06.1997.
[5] S. Knobl, G.A. Zenkovets, G.N. Kryukova, R.I. Maksimovskaya, T.V. Larina, N.T. Vasenin, V.F. Anufrienko, D. Niemeyer, R. Schlögl, Phys. Chem. Chem. Phys. 5 (2003) 5343.
[6] L.M. Plyasova, L.P. Solov'eva, S.V. Tsybulya, G.N. Kryukova, V.A. Zabolotnyi, I.P. Olen'kova, Zh. Strukt. Khim. 32 (1) (1991) 110.
[7] Y. Hu, P.K. Davies, J. Solid State Chem. 105 (1993) 489.
[8] L. Kihlborg, Arkiv Kemi 21 (1964) 427.
[9] H. Werner, O. Timpe, D. Herein, Y. Uchida, N. Pfänder, U. Wild, R. Schlögl, H. Hibst, Catal. Lett. 44 (1997) 153.
[10] G. Mestl, Ch. Linsmeier, R. Gottschall, M. Dieterle, J. Find, D. Herein, J. Jäger, Y. Uchida, R. Schlögl, J. Mol. Catal. A: Chem. 162 (2000) 455.
[11] M. Dieterle, G. Mestl, J. Jäger, Y. Uchida, H. Hibst, R. Schlögl, J. Mol. Catal. A: Chem. 174 (2001) 169.
[12] O. Ovitser, Y. Uchida, G. Mestl, G. Weinberg, A. Blume, J. Jäger, M. Dieterle, H. Hibst, R. Schlögl, J. Mol. Catal. A: Chem. 185 (2002) 291.
[13] S. Knobl, G.A. Zenkovets, G.N. Kryukova, O. Ovsitser, D. Niemeyer, R. Schlögl, G. Mestl, J. Catal. 215 (2003) 177.
[14] J.B. Wagner, D.S. Su, S.A. Schunk, H. Hibst, J. Petzoldt, R. Schlögl, J. Catal. 224 (2004) 28.
[15] T. Ushikubo, K. Oshima, A. Kayo, T. Umezawa, K. Kiyono, I. Sawaki, Mitsubishi Chem. Corp., Patent EP 529 853, publ. 03.03.1993.
[16] T. Ushikubo, Y. Koyasu, S. Wajiki, Mitsubishi Chem. Corp., Patent EP 608 838, publ. 03.08.1994.
[17] H. Hibst, F. Borgmeier, K.J. Müller-Engel, BASF Aktiengesellschaft, Patent DE 10 359 027, publ. 25.05.2005.
[18] F. Borgmeier, A. Tenten, H. Hibst, K. Müller-Engel, BASF Aktiengesellschaft, Patent WO 2002/06199, publ. 24.01.2002.
[19] F. Borgmeier, J. Petzoldt, H. Hibst, A. Tenten, BASF Aktiengesellschaft, Patent WO 2002/083615, publ. 24.11.2002.
[20] H. Watanabe, Y. Koyasu, Mitsubishi Chem. Corp., Poster, in: Fourth World Congress on Oxidation Catalysis, Berlin, 16.–21.09.2001.
[21] W. Ueda, K. Oshihara, in: Proceedings of the Fourth World Congress on Oxidation Catalysis, vol. 1, Berlin, (2001), p. 343.
[22] Y. Koyasu, Abstract of Papers, Fifth Symposium on Selective and Difficult Oxidation Catalysis, Sapporo, Japan, Organized by Catalysis Society of Japan, Tokyo, (2002/2003), pp. 11–14;
H. Tsuji, et al. Chem. Mater. 15 (11) (2003) 2112–2114.
[23] G. Cox, H. Hibst, 2002, not published.
[24] R.K. Grasselli, Catal. Today 99 (2005) 23.
[25] A.W. Sleight, Acta Chem. Scand. 20 (1966) 1102.
[26] M. Lundberg, M. Sundberg, Ultramicroscopy 52 (1993) 429.
[27] H. Hibst, Thesis, Univ. Gießen, Germany, 1977.
[28] G. Heurung, R. Gruehn, Rev. Inorg. Chem. 5 (1983) 185.
[29] T.E. Weirich, J. Porillo, G. Cox, H. Hibst, S. Nicolopoulos, Ultramicroscopy 106 (2006) 164–175.
[30] T.E. Weirich, J. Portillo, G. Cox, H. Hibst, S. Nicolopoulos, Structure determination from precession electron diffraction data, Poster, in: 10th Conference on Frontiers of Electron Microscopy in Materials Science, vol. 25, 30.09.2005, Kasteel Vaalsbroek, Netherlands.
[31] J. Barthel, T.E. Weirich, G. Cox, H. Hibst, A. Thust, Solving the missing-light-atom problem in electron crystallography via exit wave reconstruction, Poster, in: 10th Conference on Frontiers of Electron Microscopy in Materials Science, vol. 25, 30.09.2005, Kasteel Vaalsbroek, Netherlands.
[32] H. Hibst, G. Cox, F. Borgmeier, BASF Aktiengesellschaft, Patent WO 2004/099 081, publ. 18.11.2004.

[33] H. Hibst, BASF Aktiengesellschaft, S.A. Schunk, hte AG, Patent application submitted.
[34] S.A. Schunk, H. Hibst, Poster, New Cs-containing structural analogues of Mo-V-Nb-Te-O type oxides—highly prospective catalysts for the partial oxidation of methacrolein to methacrylic acid, in: Fifth World Congress on Oxidation Catalysis, Sapporo, Japan, vol. 25, 30.09.2005.
[35] E. Balcells, F. Borgmeier, I. Grißtede, H.-G. Lintz, F. Rosowski, Appl. Catal. 266 (2004) 211–221.